POWER AND ENERGY FUTURE

Open Access
Research Article

Investigation on Mixing Characteristics of Rotating Detonation Combustor with Symmetric H_2 Injection

Lei Qi, Guangyao Li, Lei Fu, Wenpeng Hong, Haoshu Ding, Xiaojuan Niu, and Guohua Wu

***Abstract*—Pressure loss in mixing process of rotating detonation combustor (RDC) acts as a critical barrier to system's pressure gain performance, thereby compromising its operational efficiency when integrated into power generation systems. Based on a symmetric H_2 injection RDC, a series of numerical simulations on mixing characteristics of RDC are conducted by altering injection position and equivalence ratio. The results show that the introduction of symmetric injection and the change of its position have a significant impact on mixing characteristic parameters, while changing equivalence ratio has little effect on mixing characteristic parameters. Counter-rotating vortex pairs (CVPs) cause an increase in non-uniformity parameters and pressure loss, as well as a decrease in detonation area ratio. As equivalence ratio decreases, total pressure recovery coefficient decreases before $x = 3.5$ mm of RDC dome and increases after $x = 3.5$ mm. At the ignition zone, when the position of nozzle moves from $x = 0$ mm to $x = -2$ mm, detonation area ratio increases from 0.318 to 0.417 and total pressure recovery coefficient increases by 1.47%.**

***Index Terms*—Rotating detonation combustor, symmetric H_2 injection, mixing performance, pressure loss.**

ABBREVIATION

RDC	rotating detonation combustor
CVP	counter-rotating vortex pair
RDE	rotating detonation engine
RD	rotating detonation
PLIF	planar laser induced fluorescence
2D	two-dimensional
NUP	non-uniformity of total pressure pulsation
LES	large eddy simulation
PISO	pressure implicit with splitting of operator
RANS	Reynolds-averaged Navier–Stokes
MUSCL	Monotone upstream-centered schemes for conservation laws
SIMPLE	semi-implicit method for pressure linked equations
JICF	jet-in-crossflow

Manuscript received 11 July, 2026; accepted 7 September, 2026. *(Corresponding authors: Haoshu Ding, e-mail: 20142511@neepu.edu.cn and Xiaojuan Niu, e-mail: nxj2018@neepu.edu.cn)*

L. Fu is with the Huaneng Tongxiang Gas-Turbine Thermal Power CO., LTD., Jiaxing 314513, China.

L. Qi, G. Li, W. Hong, H. Ding and X. Niu are with the School of Energy and Power Engineering, Northeast Electric Power University, Jilin 132012, China.

G. Wu is with the Sino-German College of Intelligent Manufacturing, Shenzhen Technology University, Shenzhen 518000, China.

Color versions of one or more of the figures in this paper are available online at https://doi.org/10.26599/PEF.2026.9650020.

Digital Object Identifier 10.26599/PEF.2026.9650020

I. INTRODUCTION

As a combustion mode in which the detonation wave continuously rotates and propagates, pressure gain characteristics [1], [2], [3] and low pollutant emissions [4] of rotating detonation combustion have always been issues of great concern in the application of gas turbines. Compared with isobaric combustion in the combustor of a traditional gas turbine, rotating detonation combustor has a higher combustion efficiency. Due to its high-pressure ratio, it can theoretically improve the overall efficiency of gas turbine. The detonation wave compresses combustible mixture through shock waves, generating instantaneous high temperature and high pressure (pressure can reach 10 to 20 times that of traditional combustion), significantly enhancing the efficiency of thermodynamic cycle. Theoretical models (such as Zeldovich cycle) show that its thermal efficiency is more than 30% higher than that of isobaric combustion.

Higashi et al. [5] and Naples et al. [6] applied rotating detonation combustion technology to the research of aero-engines and conducted various performance analyses on rotating detonation engine (RDE). Lentsch et al. [7] showed that rotating detonation engines outperform traditional rocket engines, being theoretically capable of achieving higher thermal efficiency, and indicating that this aspect is also highly beneficial for ground applications (power generation gas turbines). Liu et al. [8], [9] upgraded thermal power plants using rotating detonation combustor (RDC), achieving a superior thermodynamic cycle with RDC and modified gas turbines, and proposed a multistep optimization strategy. Through comparisons between gas turbines equipped with RDC and traditional detonation combustors, Sousa et al. [10] demonstrated the potential advantages of pressure gain combustion at low pressure ratios, with efficiency gains exceeding 5%, and indicated that the model can be used to determine the scale of small power plants. Frolov et al. [11] found that under same air pressure supply conditions, continuous rotating detonation engines can

© The author(s) 2026. Published by Tsinghua University Press.
This is an open access article under the Creative Commons Attribution 4.0 International License (http://creativecommons.org/licenses/by/4.0/).

generate greater thrust than traditional rocket engines with lower H_2 pressure supply, increasing specific impulse by 6%–8%. Wolański et al. [12] showed that applying continuous rotating detonation to GTD-350 engine under standard operating conditions can improve the engine efficiency by 5%–7%. From above studies, it can be found that pressure characteristics are of utmost importance for research and practical application of RDC. However, current existing research mainly focuses on the influence on performance, and there are deficiencies in research of RDC dome. Some studies have already mentioned the pressure gain performance of RDC without inlet mixing process.

Pressure gain performance is one of the advantages of RDE over conventional gas turbines. However, many researchers have found during their studies that RDEs do not achieve positive total pressure gain during operation. Bach et al. [13] investigated the stagnation pressure gain in RDC and its dependency on combustor geometry and mass flux, with the best-performing configuration achieving a pressure gain of −8%. Zhou et al. [14], [15], [16] found that highest total pressure gain of −15% occurs at expansion ratio = 0.87 and lower expansion ratios are required to achieve positive total pressure gain. To achieve a positive total pressure gain of RDE, a Tesla valve is introduced with intention of suppression of pressure feedback. Wen et al. [17] found that employing ideal check valve and achieving maximum inlet mass flux is the key to achieve a positive pressure gain.

Kang et al. [18] found that the intake loss while slightly diminishing combustor pressure gain capability was reduced by porous-wall RDC effectively, resulting in a marginal increase in total pressure recovery coefficient. Gray et al. [19] observed that premixed combustion and high-temperature product dilution induce a speed loss of 50% in practical RDE. Nair et al. [20] further revealed that the mixing configuration profoundly influences thermal efficiency and pressure gain, with aligned injectors demonstrating superior performance compared to misaligned setups. While increasing mass flux can enhance pressure gain, careful design is necessary to mitigate flow instabilities arising from abrupt mode transitions. Sato et al. [21] highlighted that fuel-air mixing homogeneity in RDEs directly impacts pressure gain: Inhomogeneous mixing reduces pressure amplification, and the injectors' post-detonation wave transient recovery affects stability of pressure gain characteristics. Gaillard et al. [22], [23] conducted a numerical investigation of rotating detonation (RD) propagation in a combustible mixture layer of gaseous H_2 and oxygen using large eddy simulation and injection methods, quantifying the assessment with macroscopic quantities such as RD propagation speed, average mixture parameters, and mixing efficiency. Meng et al. [24], [25] performed numerical simulations on RDC with different numbers of fuel injection holes, showing that the number of fuel holes significantly affects the formation and propagation characteristics of rotating detonation waves. Additionally, increasing the number of fuel holes can improve mixing efficiency in injection section, leading to a two-wave state in RDC and significantly enhancing thrust performance. Xu et al. [26, 27] carried out three-dimensional numerical simulations of an RDE with non-premixed injection of H_2 and air under real conditions, demonstrating that different fuel injection modes have a significant impact on engine performance. The effects of fuel injection position, injection angle, single-side or symmetric hole injection, inlet total pressure, and outlet back-pressure on cold-flow mixing effect at RDC dome were investigated. Rankin et al. [28] studied fuel-air mixing process in a non-premixed RDE using acetone planar laser induced fluorescence (PLIF) technique, observing a recirculation zone with the lowest fuel concentration at outer corner of annular deflagration channel near the fuel injection surface, and identifying key design parameters affecting RDE operation and performance. In above researches, investigations were focused on the evolution of hot flow field in RDC dome, however, the analysis of cold flow field mixing characteristics remains incomplete.

Driscoll et al. [29], [30], [31] carried out a two-dimensional numerical study on mixing process and flow field characteristics of fuel and oxidizer at RDC dome. They analyzed different injection parameters for the mixing mechanism and studied the flow field recirculation area by changing injection area. In subsequent studies, they fully verified results through three-dimensional numerical simulation and found that increasing the number of fuel injection holes can improve mixing degree, but there is an optimal number of fuel injection holes to achieve best mixing degree. Weiss et al. [32] provided three main flow characteristics in their research to analyze mixing process: supersonic shock mode, two main recirculation zones, and counter-rotating vortex pair (CVP) structure. Through a parametric study of nine different flow configurations, they analyzed the effects on mixing behavior and performance to determine parameters that have the greatest impact on RDC filling process.

In RDC, after air is accelerated through convergent section to reach the sonic velocity flow, it collides with longitudinal H_2 jet, and the shedding and fragmentation of vortex system structure occur at RDC dome. Therefore, adopting mixing enhancement technology to achieve the rapid and uniform mixing of fuel and air is a significant issue that urgently needs to be solved at present. Ben Ali et al. [33] found that fuel mixing has been increased when air jet is injected since the interaction flow is higher via internal airflow in a supersonic combustion chamber. Chong et al. [34] found that from the first multiple necklace-like vortex onward, dominant vortex structures develop separately in upper and lower layers until flow runs into the fully developed turbulent state. Huang et al. [35] found that the forced excitation of large-scale vorticity is utilized to improve mixing efficiency between fuel and air for active mixing augmentation devices. Sun et al. [36] revealed that increasing jet pressure decreases fuel mixing of jets released from backward-facing steps in the performance of hyper/supersonic vehicles. Li et al. [37] found that the growth of amplitude of sinusoidal shock generator could augment the

mixing of fuel jet with a supersonic mainstream inside combustor.

In the previous work of Qi et al. [38], the mixing characteristics of an RDC with single-side H_2 injection were numerically investigated. However, the limited penetration of the single-side H_2 jet restricts its transport across the combustor, and the influence of symmetric injection on the mixing process remains unclear. To address this issue, the present study adopts a symmetric H_2 injection configuration and systematically investigates the effects of injection arrangement, injection position, and equivalence ratio (Eq, defined as the ratio of the fuel–oxidizer ratio of the actual mixture to the fuel–oxidizer ratio of the stoichiometric mixture) on the non-reacting mixing characteristics of the RDC. Particular attention is paid to the changes in H_2 penetration, vortex development, mixture distribution, and total-pressure loss induced by symmetric injection. The present work therefore extends the previous single-side injection study by clarifying the coupled influence of symmetric fuel injection on mixture preparation and aerodynamic loss.

II. Numerical Simulation Methods

A. Computational model

Figure 1(a) shows sectional view of a symmetric H_2 injection RDC model. The cylindrical RDC defines the central point of its inlet plane as coordinate origin, with axial direction as positive x-direction, and inlet cross-section is located at x = 0 mm. In this study, research and analysis are conducted by sectioning a 1/60 circumferential sector of the complete annular RDC, and Fig. 1(b) presents schematic diagram of sectioned two-dimensional (2D) plane. This 2D RDC is a symmetric model, and the distance from its symmetric centerline to axis of overall RDC is 15 mm. Specifically, the width of air inlet is 4.5 mm, the widths of hydrogen inlets on both sides are each 0.035 mm, and the width of RDC itself is 1.5 mm. The H_2 injection position of model shown in Fig. 1(b) is at x = 0 mm. For purposes of this study, the direction toward inlet of convergent section is defined as the negative direction, while

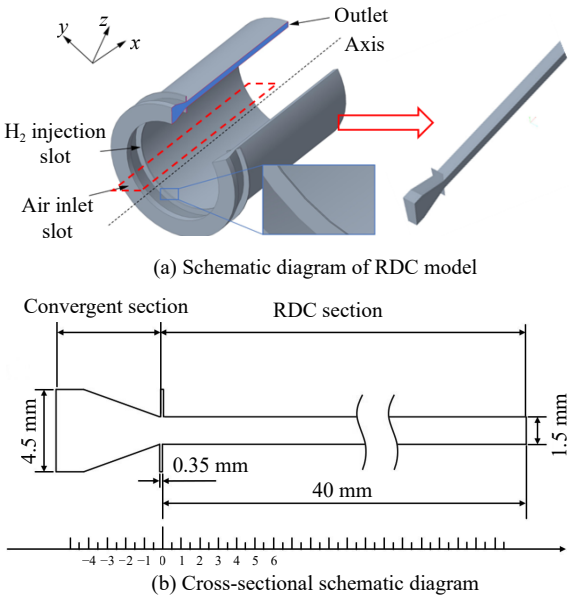

(a) Schematic diagram of RDC model

(b) Cross-sectional schematic diagram

Fig. 1. Section view of RDC.

the direction toward outlet of RDC is defined as the positive direction. Additionally, the range of axial direction from x = 0 mm to x = 11 mm is designated as RDC dome.

Air inlet and hydrogen inlet adopted mass flow rates inlet boundary. Total temperature was 300 K for both. RDC outlet was pressure outlet boundary, and outlet pressure was P_b = 0.1 MPa. To further analyze mixing characteristics of RDC with symmetric H_2 injection ports, different H_2 injection methods and inlet conditions of air and H_2 into different conditions were summarized in this paper, as shown in Table 1.

B. Mixing characteristic parameters

To present a more thorough description of mixing process between H_2 and air, a parameter named "mixing non-uniformity" was introduced to characterize the mixing performance of reactants within RDC. It was defined as follows

$$s = \sqrt{\sum_{i=1}^{n} \left(\gamma_i^* - \gamma_{i,\,\mathrm{ave}}^*\right)^2 / (n-1) / \gamma_{i,\,\mathrm{ave}}^*} \tag{1}$$

TABLE 2
SUMMARY OF WORKING CONDITIONS

Working conditions	Nozzle numbers	H_2 injection position	Air mass flow rate	Equivalence ratio
Case 1-1	2	x = −2 mm	1.55 kg/s	1
Case 1-2	1	x = −2 mm	1.55 kg/s	1
Case 1-3	2	x = 0 mm	1.55 kg/s	1
Case 1-4	1	x = 0 mm	1.55 kg/s	1
Case 2-1	2	x = −0.5 mm	1.55 kg/s	1
Case 2-2	2	x = −1 mm	1.55 kg/s	1
Case 2-3	2	x = −1.5 mm	1.55 kg/s	1
Case 3-1	2	x = −2 mm	1.55 kg/s	0.8
Case 3-2	2	x = −2 mm	1.55 kg/s	0.6

where γ_i^* is the mass fraction of H_2 at each grid point on the cross-section perpendicular to RDC, and $\gamma_{i,\text{ave}}^*$ is the average mass fraction of H_2 on cross-section. The mixing non-uniformity characterizes the spatial uniformity of the H_2 distribution over a given cross-section, and a smaller value indicates a more homogeneous H_2/air mixture.

In order to further research mixing characteristics, the upper and lower limits of H_2/O_2 detonation equivalence ratio obtained by Zhou et al. [39] were 0.2 and 3.2, with corresponding H_2 mass fractions of 0.0056 and 0.0906, respectively. Based on the equation in the research of Zhao and Zhang [40], the ratio of range satisfying detonation equivalence ratio to entire cross-sectional area was analyzed to characterize detonation area ratio, which was defined as φ

$$\varphi = \frac{\int \gamma \mathrm{d}A}{\int \mathrm{d}A},\ \gamma = \begin{cases} 1, & \text{if } 0.0056 < \gamma_i^* < 0.0906 \\ 0, & \text{otherwise} \end{cases} \tag{2}$$

where γ_i^* is the mass fraction of H_2, and A is the section unit grid range. It should be noted that the detonation area ratio used in the present non-reacting study is a composition-based indicator. It represents the fraction of the cross-sectional area in which the local H_2 concentration falls within the prescribed detonable composition range and does not imply the occurrence of actual detonation.

In detonation combustion field, contact discontinuity surface contains unstable vortices or curvature change points formed by degradation of these vortices, which cause oscillations in combustor intake mass flow rate and ultimately lead to variations in cross-sectional parameters. Therefore, this paper analyzes non-uniformity of total pressure pulsation across different cross-sections of RDC under various operating conditions. Non-uniformity of total pressure pulsation (NUP) is calculated as follows

$$\text{NUP} = \sqrt{\sum_{i=1}^{n} \left(P_i^* - P_{i,\text{ave}}^*\right)^2 / (n-1)} / P_{i,\text{ave}}^* \tag{3}$$

where P_i^* and $P_{i,\text{ave}}^*$ are the total pressure of each grid point on cross-section and average total pressure of whole cross-section, respectively, and n was a number of grid points within statistical range.

To better characterize variation in total pressure loss across each cross-section of RDC, a total pressure recovery coefficient σ was introduced, defined such that a larger σ value indicates smaller total pressure loss in a specific section, while a smaller σ value signifies greater total pressure loss. This coefficient is defined as

$$\sigma = P_{i,\text{ave}}^* / P_0^* \tag{4}$$

where P_0^* is the average total pressure of air inlet.

C. Grid independence verification and model validation

According to previous research by our team [38], data from different maximum grid sizes show that the error between fine meshes 1 and 2 in Fig. 2 does not exceed 1%. Therefore, fine mesh 1 suffices for the computational requirement.

For grids employed in this simulation, their detailed information is presented in Table 2.

As a high-precision turbulent flow analysis method, large

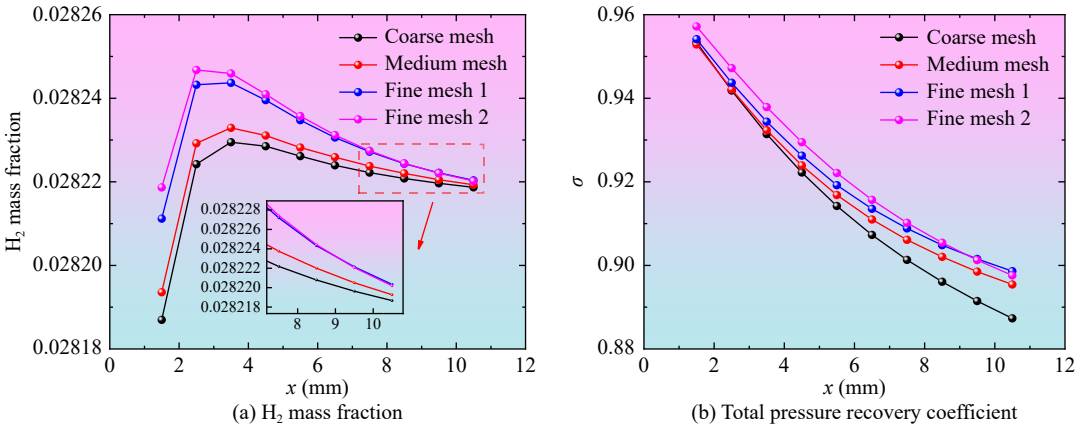

Fig. 2. Grid independence verification.

TABLE 3
THE DETAILED INFORMATION OF MESH GENERATION

	Max element	H_2 injection hole
Coarse mesh	0.20 mm	0.003 mm
Medium mesh	0.15 mm	0.003 mm
Fine mesh 1	0.10 mm	0.003 mm
Fine mesh 2	0.08 mm	0.003 mm

eddy simulation (LES) has demonstrated strong applicability in the study of compressible flows. In this paper, a LES model was constructed based on the assumption of an ideal compressible fluid, and a pressure-based solver coupled with pressure implicit with splitting of operator (PISO) algorithm was adopted to iteratively solve Navier–Stokes equations. To verify the model's accuracy, physical model and numerical method used in the research of Zhou et al. was selected for comparative verification in this study. Figure 3 presents the results of H_2 mass fraction distribution during mixing process of H_2 and air simulated in this paper. LES-calculated H_2 mass fraction contours are in good agreement with numerical results of Zhou et al. [39], and H_2 injection depth and its axial distribution in combustor are basically consistent, preliminarily verifying the reliability of numerical model in this paper.

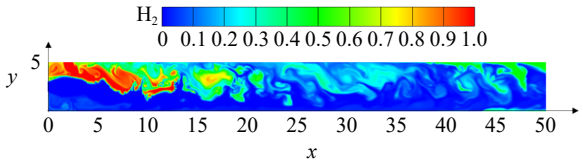

(a) Hydrogen mass fraction contour of this calculation method

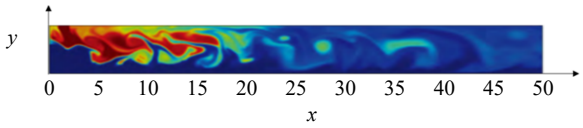

(b) Hydrogen mass fraction contour in the study of Zhou et al. [39]

Fig. 3. Comparison of H_2 mass-fraction distributions for LES validation.

In this study, Reynolds-averaged Navier–Stokes (RANS) simulation method for steady-state compressible flow based on unstructured grids was adopted. Mixing characteristics of hydrogen and air in RDC were investigated using ANSYS Fluent software. The discretization of convective terms was implemented with third-order Monotone upstream-centered schemes for conservation laws (MUSCL). To accurately characterize the jet behavior in crossflow, this study employs a pressure-based steady-state solver: The standard k–ε turbulence model is adopted to close Reynolds stresses, the species transport model tracks the interaction between jet and mainstream, and pressure and velocity are coupled by the semi-implicit method for pressure linked equations (SIMPLE) algorithm. This steady-state RANS framework has been shown to agree closely with experimental data in jet-in-crossflow (JICF) simulations, providing a reliable foundation for the present numerical investigation. To verify accuracy of the model in this paper, Fig. 4 shows H_2 mass fraction contours obtained using the numerical method in this study, and its numerical simulation results are very close to those of Driscoll et al. [30]

III. Calculation Results and Analysis

A. Analysis of mixing characteristics between single-side H_2 and symmetric H_2 injection

As shown in Fig. 5(a), at x = −2 mm, mixing non-uniformity curve of case 1-2 is relatively stable, while mixing non-uniformity curve of case 1-1 (2 nozzles, x = −2 mm, 1.55 kg/s, Eq = 1) shows a gradually decreasing trend. In addition, the curve of case 1-1 is lower than that of case 1-2 (1 nozzle, x = −2 mm, 1.55 kg/s, Eq = 1) after x = 7.5 mm. Although the initial mixing performance of case 1-1 is lower than that of case 1-2, the mixing performance of case 1-1 improves rapidly along axial direction of RDC and is better than that of case 1-2 in last two sections. At x = 0 mm, the initial mixing non-uniformity of case 1-3 (2 nozzles, x = 0 mm, 1.55 kg/s, Eq = 1) is much greater than that of case 1-4 (1 nozzle, x = 0 mm, 1.55 kg/s, Eq = 1). In addition, the mixing non-uniformity value of case 1-3 drops rapidly from 11 and finally becomes the same as that of case 1-4 at the position of x = 10.5 mm, while case 1-4 is relatively stable. These results indicate that 2-nozzle structure will lead to unsatisfactory mixing performance in a short distance within RDC, but it can rapidly improve mixing performance in the range of x = 9.5–10.5 mm and finally achieve the same mixing performance as that of 1-nozzle structure.

As shown in Fig. 5(b), the detonation area for four structures all show an upward trend. Detonation area ratio of case 1-2 increases uniformly from 0.1 to 0.5 along axial direction of RDC. In addition, detonation area ratio of case 1-1 at the initial position is larger than that of case 1-2, and detonation area ratio increases rapidly along axial direction of RDC at the position of x = 6–8 mm. However, the rising rate slows down after the position of x = 9.5 mm, but the final value reaches 1, which is nearly twice the final value of case 1-2 at same posi-

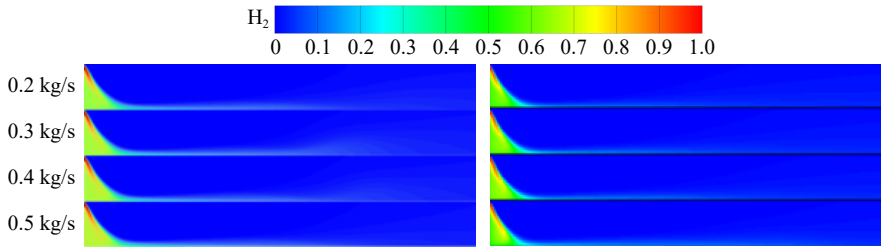

(a) Hydrogen mass fraction contour of this calculation method

(b) Hydrogen mass fraction contour in the study of Driscoll et al. [30]

Fig. 4. Comparison of H_2 mass-fraction distributions for RANS validation.

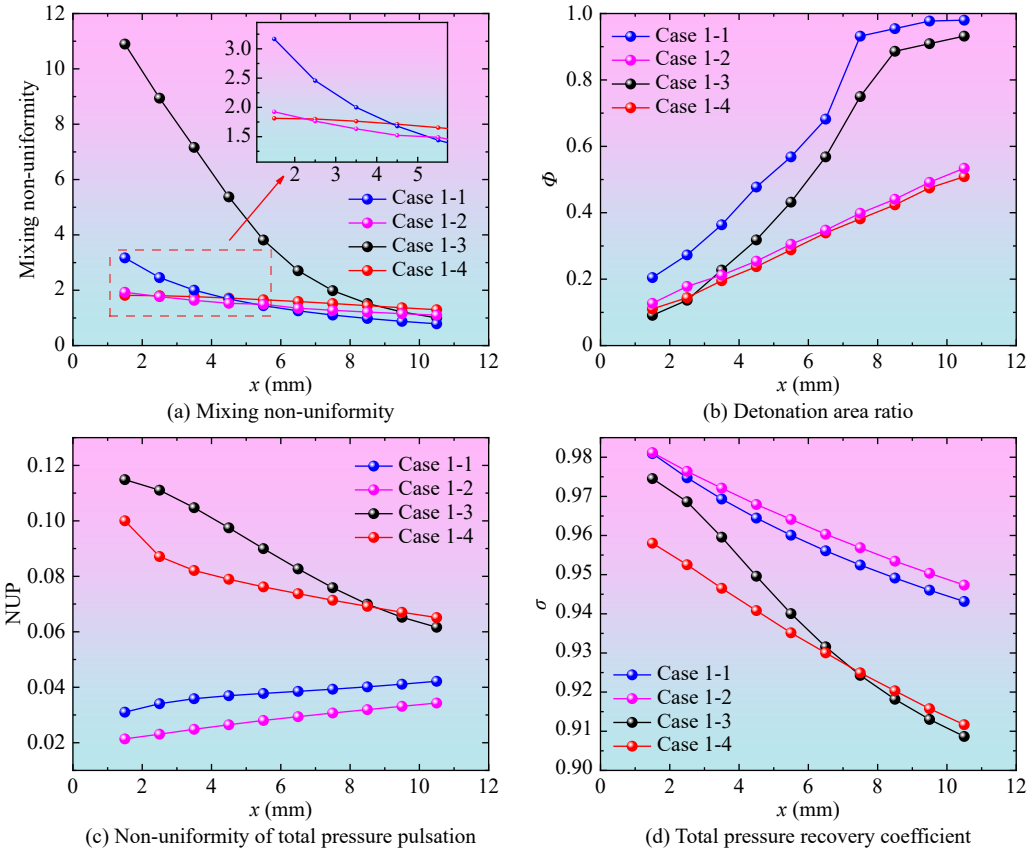

Fig. 5. Axial distributions of mixing-characteristic parameters for different H_2 injection arrangements.

tion. At x = 7.5 mm, detonation area ratio increases from 0.40 to 0.93 with symmetric H_2 injection. Among them, the value of case 1-4 shows a linear upward trend along axial direction of RDC. The value of case 1-3 is lower than that of case 1-4 at the initial position, but it exceeds that of case 1-4 after x = 2.5 mm. Detonation area ratio of case 1-4 increases from 0.1 to 0.51, while detonation area ratio of case 1-3 increases rapidly. The rising rate slows down after the position of x = 9.5 mm, but final value reaches 0.93, which is nearly twice compared to that of case 1-4. In the ignition region of RDC, detonation area ratio of case 1-3 is significantly higher than that of case 1-4.

As shown in Fig. 5(c), the values of each section of case 1-1 are greater than those of case 1-2. This result indicates that total pressure stability of both cases 1-1 and 1-2 gradually weakens along axial direction of RDC. Although H_2 is injected bilaterally, numerically, NUP is relatively low when H_2 is injected in convergent section. At the initial position, the value of case 1-3 is higher than that of case 1-4. However, along axial direction of RDC, the curve of case 1-3 decreases with a faster rate. NUP value of case 1-3 drops below that of case 1-4 after the position of x = 8.5 mm.

As shown in Fig. 5(d), along axial direction of RDC, the values of case 1-1 are all smaller than those of case 1-2, and difference gradually increases. It can be seen that in the ignition region, total pressure loss of case 1-1 is slightly greater than that of case 1-2, and total pressure recovery coefficient of case 1-2 is 0.5% larger than that of case 1-1. The curve descending rate of case 1-3 is greater than that of case 1-4. Therefore, after x = 7.5 mm, the curve of case 1-3 is lower than that of case 1-4 and remains so until the position of x = 10.5 mm. Thus, overall total pressure loss of case 1-3 is greater than that of c ase 1-4. After the ignition region of RDC, total pressure recovery coefficient curves of cases 1-3 and 1-4 are very close.

Figure 6 shows a comparison of Mach Number contours of RDC for four cases. In convergent section of case 1-1, there is only a small area near H_2 inlet where Mach number reaches 1. After outlet of convergent section, parts with a Mach number exceeding 1 gradually appear near the two side walls, and they develop axially along RDC in a wavy shape. At downstream of RDC, the flow field area with a Mach number exceeding 1 accounts for most of entire flow field. The mixing non-uniformity value of case 1-1 will gradually decrease and be lower than that of case 1-2 along axial direction of RDC, mixing performance of case 1-1 is better than that of case 1-2. In case 1-2, there is a section where Mach number exceeds 1 after H_2 inlet, and the area where Mach number exceeds 1 at downstream of convergent section is also significantly larger than that of case 1-1. In downstream flow field of RDC, area with Mach number exceeding 1 occupies the vast majority. As shown in the figure, the red part represents where Mach num-

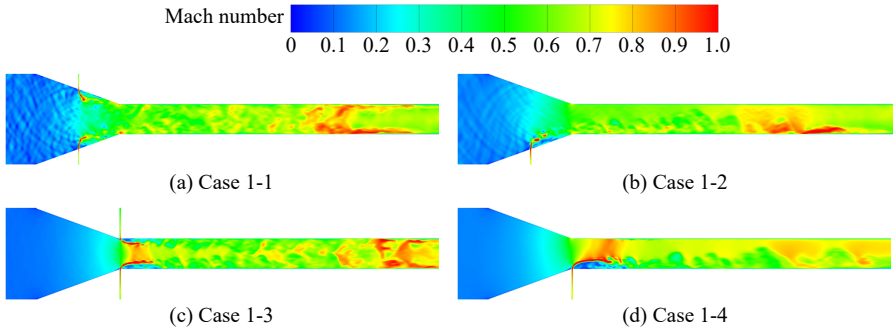

Fig. 6. Mach number contours for different H_2 injections.

ber is above 1. For case 1-3, these areas concentrate at H_2 injection inlet and RDC rear end, with no supersonic flow in the middle. Moreover, Mach number is approximately 0.5 near the positions close to two side walls, and there are several small areas where Mach number is around 0.1. In case 1-4, most of areas inside reach a Mach number of 1 or even exceed 1. Different from case 1-3, the area with a Mach number exceeding 1 almost fills entire RDC. Compared with case 1-4, the distribution of Mach number in case 1-3 is relatively uniform and symmetrical, and most of values are below 1. Although the mixing non-uniformity of case 1-3 is not as good as that of case 1-4 in early stage, it can achieve the same H_2 mixing non-uniformity in a short time, and it performs better in terms of detonation area ratio value. Therefore, its mixing performance is better.

Figure 7 displays H_2 mass fraction on Q-criterion isosurface ($Q = 10^{10}$). Horseshoe vortices of symmetric H_2 injection are distributed near H_2 annulus in a scattered pattern, while those of single-side H_2 injection are distributed along radial direction of RDC in a banded pattern. Hanging vortices are distributed in the downstream region of H_2 injection port. Those of cases 1-1 and 1-2 are located at convergent section outlet and RDC dome, while those of cases 1-3 and 1-4 are distributed at the central position of RDC. In configuration with symmetric H_2 injection, hovering vortices are distributed along inner and outer wall surfaces of RDC. Specifically, H_2 mass fraction inside hovering vortices ranges from 0.4 to 0.6 for case 1-1, and it is about 0.8 for case 1-3. CVP is distributed where hydrogen is adjacent to RDC wall; recirculation zones appear only in axial direction but not in the circumferential direction, with hydrogen mass fraction ranging from 0.3 to 0.6.

Figure 8 shows a comparison of velocity streamline contours of cases 1-1, 1-2, 1-3, and 1-4. It can be seen that the change of velocity in the flow field is mainly caused by H_2 injection. There is three small recirculation zone on inner and outer side of case 1-1, while due to penetration depth and velocity of H_2, case 1-2 has two small recirculation zones. When injecting from a single nozzle, H_2 entering convergent section mainly affects flow field on one side. Injecting from double nozzles affects flow fields on both sides simultaneously. Although the penetration depth and velocity of H_2 in case 1-1 are smaller than those in case 1-2, during the acceleration process of gas in convergent section, it has a greater impact on flow field. This also makes NUP and total pressure loss at RDC dome in case 1-1 larger. Due to insufficient penetration depth of H_2 in case 1-3, one recirculation zone is generated near the H_2 injection inlet on each side of RDC. The H_2 in case 1-4 has a relatively large penetration depth and a high velocity after injection, and three recirculation zones are

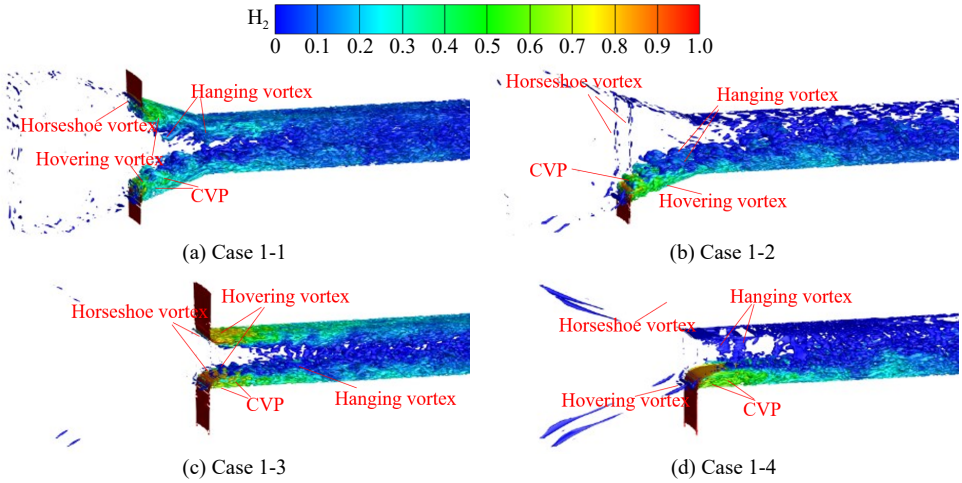

Fig. 7. H_2 mass fraction in terms of Q-criterion isosurface ($Q = 10^{10}$) of different H_2 injections.

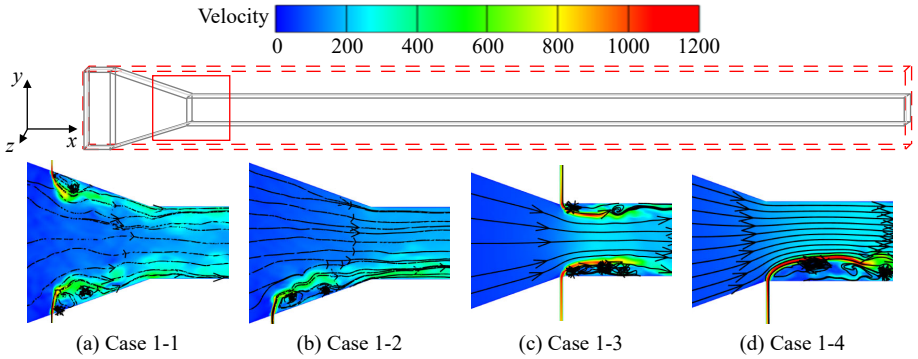

Fig. 8. Velocity streamline contours for different H_2 injections at $z = 0$ mm.

formed. Although velocity distribution in flow field of RDC is more uniform, this injection structure makes H_2 mixing non-uniformity of H_2 at RDC dome significantly greater than that of case 1-4. In contrast, the velocity distribution of flow field inside case 1-4 is less uniform, and total pressure recovery coefficient is slightly lower than that of case 1-3. Since H_2 in case 1-4 has a greater penetration depth in flow field, NUP is significantly smaller than that of case 1-3.

Figure 9 shows the velocity distribution contours at different heights of RDC. Since hydrogen is injected into the flow field at a relatively high velocity, it can be seen that at combustor height of $y = 15$ mm, the velocity distributions of two injection configurations are nearly identical, and the flow field velocity is notably lower than those at heights of $y = 15.375$ and 14.625 mm. In H_2 single-side injection configuration, the velocity at inner wall of RDC is significantly higher than that at outer wall, and the velocity in downstream of combustor reaches 400 m/s. Symmetric H_2 injection contributes to a more uniform velocity distribution along radial direction of the flow field, with high-velocity regions concentrated near inner and outer wall surfaces.

B. Analysis of mixing characteristics for different H_2 injection positions

Based on above research, it can be found that the structure of double H_2 injection will endow RDC with a convergent inlet with more excellent mixing performance. Although mixing performance in terms of total pressure recovery coefficient is not ideal, it is still within a reasonable range. Therefore, the subsequent research will also be carried out based on the structure of double H_2 injection.

As shown in Fig. 10(a), H_2 mixing non-uniformity of five structures shows a downward trend. At the initial cross-section, as H_2 injection position moves forward, the value of H_2 mixing non-uniformity gradually decreases. The descending curves of H_2 mixing non-uniformity of five working conditions all maintain this variation pattern and tend to approach 1 at the position of $x = 10.5$ mm. As injection position moves forward, the descending rate of H_2 mixing non-uniformity gradually becomes smaller. The results show that mixing performance of case 1-1 is the best, and the closer H_2 injection position is to inlet position of convergent section, the better mixing performance is.

As shown in Fig. 10(b), the variation curves of detonation area ratio for five structures all show an upward trend. During the upward process of five curves, the numerical variation patterns of five conditions at the same cross-section basically remain that the value of case 1-1 is the largest and that of case 1-4 is the smallest. As H_2 injection position moves forward, detonation area ratio at the same position of RDC is larger. This suggests that the nearer H_2 injection nozzle is to inlet of convergent section, the superior mixing performance will be.

As shown in Fig. 10(c), the NUP curve of case 1-3 is significantly different from NUP curves of other four conditions. The NUP variation curve of case 1-3 is significantly larger than those of other four conditions at $x = 0$ mm. The curves of other four conditions show a gradually decreasing trend. The variation curve of case 2-1 (2 nozzles, $x = -0.5$ mm, 1.55 kg/s, Eq =

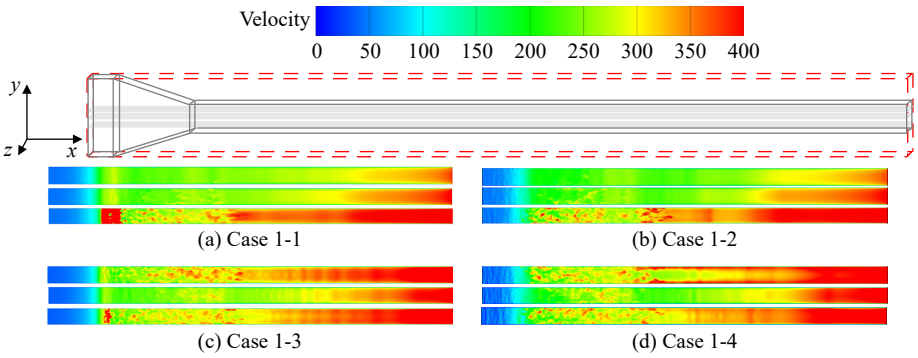

Fig. 9. Velocity contours for different H_2 injections at $y = 15.375$, 15 and 14.625 mm.

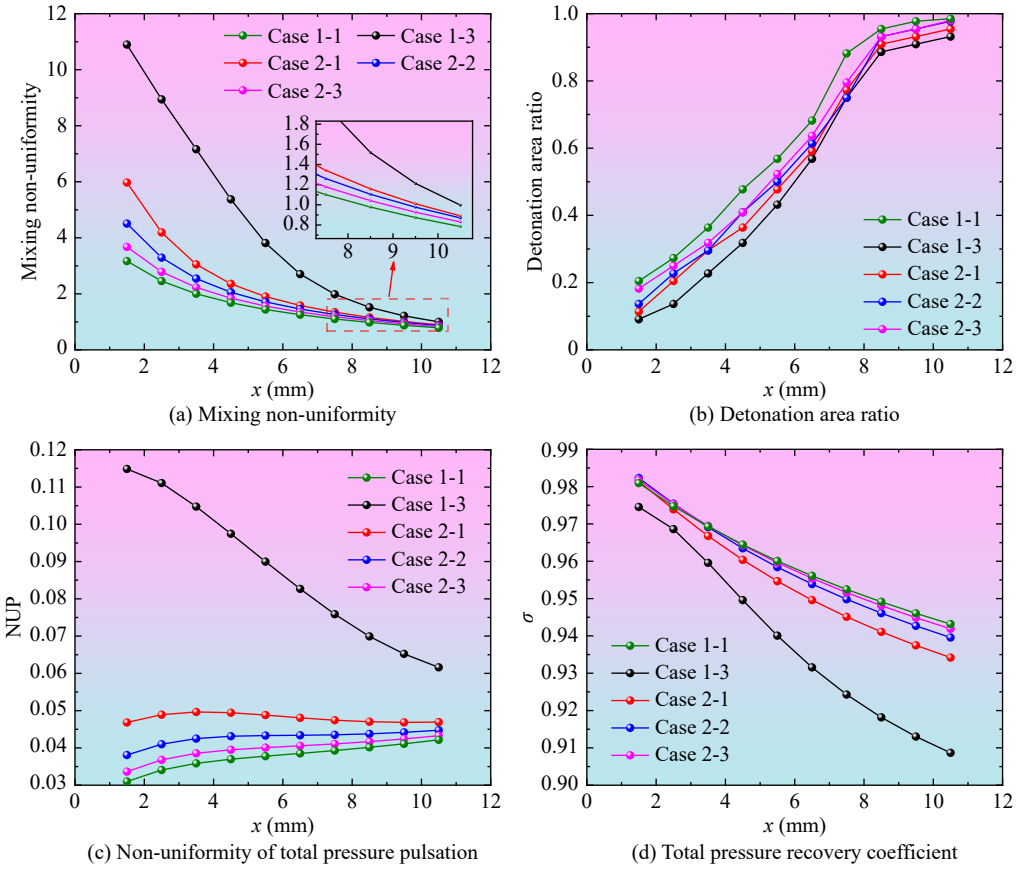

Fig. 10. Axial distributions of mixing-characteristic parameters for different H_2 injection positions.

1) shows an upward trend at x = 1.5–3.5 mm, and a downward trend after x = 3.5 mm, and finally levels off. The variation curves of cases 1-1, 2-2 (2 nozzles, x = −1 mm, 1.55 kg/s, Eq = 1), and 2-3 (2 nozzles, x = −1.5 mm, 1.55 kg/s, Eq = 1) have a very small upward trend. In addition, at each cross-section, the NUP value gradually decreases as the position of H_2 injection nozzle moves towards inlet position of convergent section. Therefore, among these five working conditions, when H_2 injection nozzle is at the position of x = −2 mm, total pressure pulsation non-uniformity is the smallest. Since hydrogen nozzle is located at RDC dome, the H_2 jet collides with incoming air flow at this point, leading to intense pressure fluctuations. The other four cases have already formed a vortex structure in convergent section, so pressure fluctuations tend to be uniform at RDC dome.

As shown in Fig. 10(d), total pressure recovery coefficient curves of five structures all show a gradually decreasing trend. Among them, the variation curve of case 1-3 is significantly different from those of other four conditions. Firstly, total pressure recovery coefficient at initial position is approximately 0.975, which is significantly smaller than those of other four conditions. In addition, descending rate of curve is greater after x = 2.5 mm. Moreover, it can be seen that total pressure recovery coefficient gradually increases as the position of H_2 injection nozzle moves towards inlet of convergent section, indicating that when the position of H_2 injection nozzle is at x = −2 mm, total pressure recovery coefficient is the largest, and total pressure loss is the smallest.

In the ignition zone (RDC at x = 4.5 mm), H_2 mixing non-uniformity decreases from 5.37 to 1.68, total pressure recovery coefficient increases by 1.47% and detonation area ratio increases from 0.318 to 0.417.

Figure 11 shows Mach number contours when H_2 injection positions are at x = −2, −1, and 0 mm. It can be found that different H_2 injection positions will lead to significant differences in Mach number distribution in flow field. When H_2 injection position is at x = −2 mm, H_2 is injected into the flow field through injection nozzle and mixes with air. After the mixed gas is accelerated, it flows out of convergent section. In cases 1-1 and 2-2, along radial direction, the velocity gradually decreases from both sides of inner and outer wall surfaces towards the middle. In downstream of flow field, the velocity of entire flow field is close to Mach 1. In case 1-3, a sonic region appears at H_2 injection position and is concentrated in the middle of RDC. However, the positions close to inner and outer wall surfaces are in a beaded subsonic state. At downstream of RDC, the sonic region gradually expands, and the flow field on inner and outer wall surfaces of RDC also reaches the state of sonic flow. Therefore, it can be proved that flow field formed by the injection structure with H_2 injection position in convergent section makes mixing performance better, and moving the injection position towards inlet position of

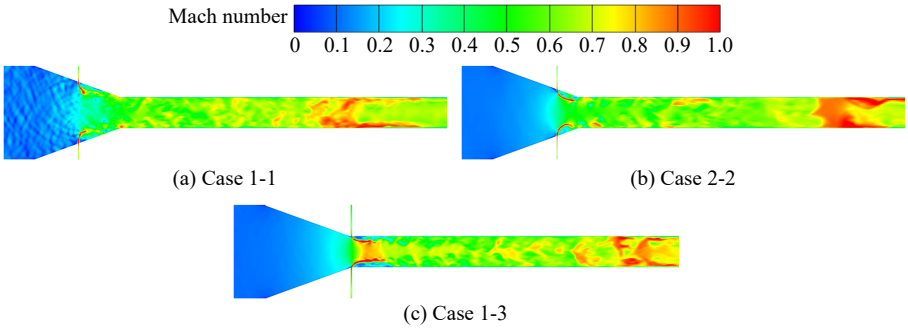

Fig. 11. Mach number contours of different H_2 injection positions at $z = 0$ mm.

convergent section will gradually enhance mixing performance.

Figure 12 displays H_2 mass fraction on Q-criterion isosurface ($Q = 10^{10}$) of different H_2 injection positions. At different H_2 injection positions, horseshoe vortices exhibit a scattered distribution adjacent to H_2 injection ports. Trailing vortices are localized at RDC dome, where the H_2 mass fraction is approximately 0.1. CVPs are distributed on both inner and outer walls of RDC, and the formation of recirculation zones in these regions can be clearly observed in Fig. 13. Downstream of CVP, hovering vortices attach to inner and outer wall surfaces of RDC, with the corresponding H_2 mass fraction ranging from 0.6 to 0.8. CVP plays a significant role in mixing characteristics of flow field, resulting in increased mixing nonuniformity and NUP, as well as decreased detonation area ratio and total pressure recovery coefficient.

Figure 13 shows a comparison of the velocity streamline contours of cases 1-1, 2-2, and 1-3. It can be seen that the change of velocity in flow field is mainly caused by H_2 injection. There is three small recirculation zone on inner and outer

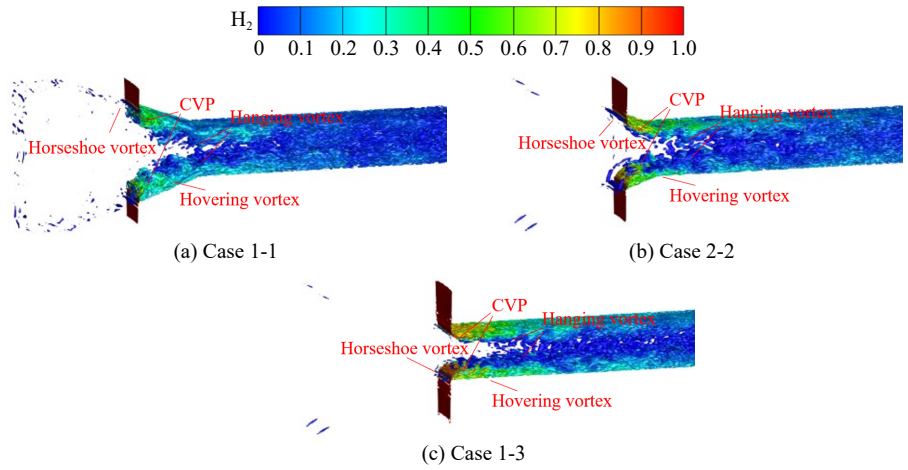

Fig. 12. H_2 mass fraction in terms of the Q-criterion isosurface ($Q = 10^{10}$) of different H_2 injection positions.

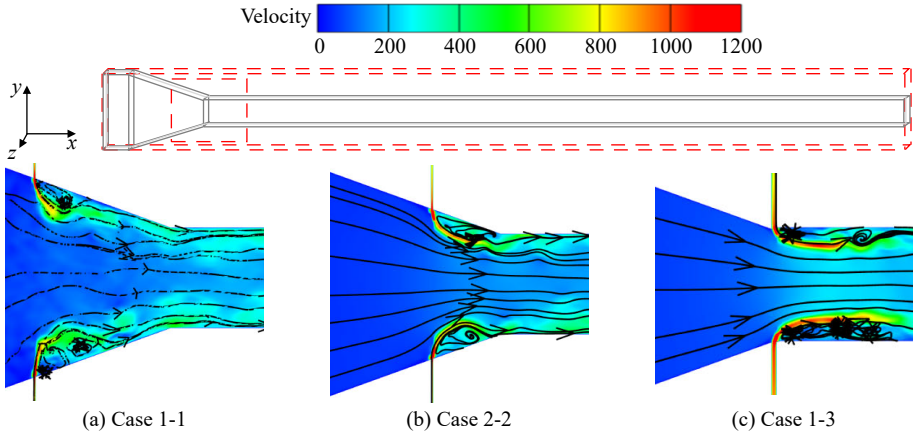

Fig. 13. Velocity streamline contours of different H_2 injection positions at $z = 0$ mm.

side of case 1-1, while due to the penetration position, case 2-2 has two small recirculation zones. When injecting at $x = -2$ mm, there is an obvious enlargement in the range of recirculation zone. Notably, the flow velocity within recirculation zone reaches up to 800 m/s, while the maximum velocity in flow field reaches as high as 1200 m/s.

Figure 14 shows the velocity distribution contours at different heights of RDC. With H_2 being injected into flow field at a relatively high speed, the velocity profiles of two injection schemes are highly consistent at combustor height of y = 15 mm, whereas the corresponding flow field velocity is markedly lower than those at y = 15.375 and 14.625 mm. Combined with Fig. 10, as H_2 injection position gradually shifts from convergent section to RDC dome, mixing performance of combustor deteriorates progressively, and total pressure loss increases accordingly.

C. Analysis of mixing characteristics for different equivalence ratios

Mixing characteristics with different reactant equivalence ratios are conducted in this section when mass flow rate of air inlet is fixed.

As shown in Fig. 15(a), the overall H_2 mixing non-uniformity under three conditions shows a downward trend, and

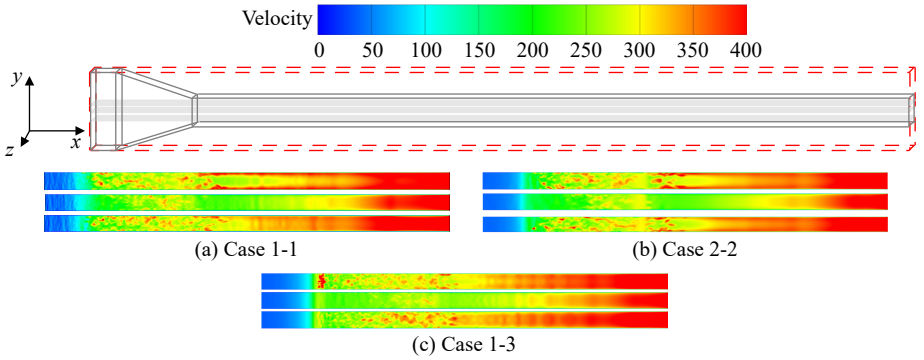

Fig. 14. Velocity contours of different H_2 injection positions at y = 15.375, 15, and 14.625 mm.

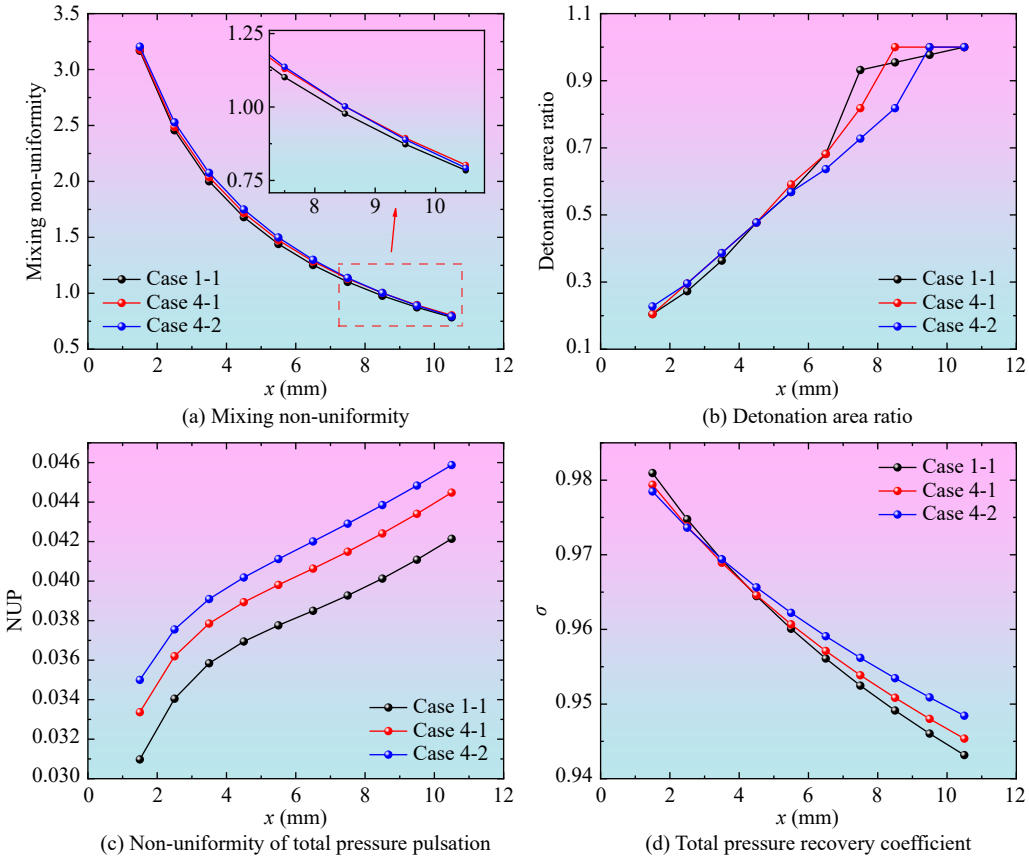

Fig. 15. Axial distributions of mixing-characteristic parameters at different equivalence ratios.

mixing performance gradually improves. Curves of H_2 mixing non-uniformity vary little under different equivalence ratios. At the same cross-section, it can be found that as equivalence ratio decreases, H_2 mixing non-uniformity increases, and mixing performance decreases. However, at the position of x = 10.5 mm, H_2 mixing non-uniformities of three conditions are consistent.

As shown in Fig. 15(b), detonation area ratio under three conditions shows an upward trend. However, during the upward process, curves of three conditions do not change completely regularly. Case 3-2 (2 nozzles, x = −2 mm, 1.55 kg/s, Eq = 0.6) has the best detonation area ratio before x = 4.5 mm, but shows a relatively poor detonation area ratio after x = 4.5 mm. Cases 1-1 and 3-1 (2 nozzles, x = −2 mm, 1.55 kg/s, Eq = 0.8) have the best detonation area ratio among three conditions at x = 7.5 and 8.5 mm, respectively. In addition, when at the position of x = 10.5 mm, detonation area ratios of three conditions all reach 1.

As shown in Fig. 15(c), the NUP curves under three conditions show obvious changes. All three curves exhibit an upward trend. However, at the same cross section, a lower equivalence ratio corresponds to a higher NUP value and more intense pulsation amplitude of total pressure.

As shown in Fig. 15(d), overall curves of total pressure recovery coefficient under three conditions shows a downward trend. At the initial position, total pressure recovery coefficient at the same cross-section decreases with the decrease of equivalence ratio. However, after the position of x = 3.5 mm, the situation is opposite. At the same cross-section, total pressure recovery coefficient increases with decrease of equivalence ratio, and the difference gradually increases as axial depth of RDC increases. With the increase of equivalence ratio, the momentum of hydrogen jet increases, forming larger-scale turbulent vortex structures with the incoming oxygen flow at RDC dome. This leads to a decrease in total pressure recovery coefficient before axial position of x = 3.5 mm. However, an increase in equivalence ratio reduces the influence of incoming oxygen flow on hydrogen jet, which in turn causes the downward trend of total pressure recovery coefficient to gradually slow down. After the position of x = 3.5 mm, total pressure recovery coefficient becomes larger.

Figure 16 shows Mach number contours under different equivalence ratios, and conditions are cases 1-1, 3-1, and 3-2. It can be found that the distribution of sonic region and supersonic region is similar, but Mach number at each position in RDC is weakened as equivalence ratio decreases. At the same time, Mach number in the front section of RDC decreases, and its NUP value increases. Combined with Fig. 15, as the flow velocity decreases, pressure loss reduces after the mixing process of air and H_2, while total pressure fluctuation becomes more intense.

Figure 17 shows H_2 mass fraction contours under different equivalence ratios. It can be found from the figure that as equivalence ratio decreases, the penetration depth of H_2 decreases, and after H_2 enters RDC, it will flow closer to wall surface. In RDC dome, slight disturbances of H_2 can be observed in all three conditions, which also makes H_2 mixing non-uniformity in the front section of RDC basically the same. In addition, the structure of symmetric H_2 injection enables detonation area ratio to completely reach the ideal value of 1 after x = 10.5 mm. Even equivalence ratio decreases, detonation area ratio will eventually reach 1. Vortex structures of cases 1-1, 3-1, and 3-2 are essentially identical. Horseshoe vortices are distributed adjacent to hydrogen injection ports, while CVPs are located on inner and outer sides of RDC convergent section.

Figure 18 shows the comparison of velocity vortex streamline contours under different equivalence ratios. It can be clearly found that the decrease of equivalence ratio will lead to insufficient penetration depth of H_2, and at the same time, recirculation zones at H_2 inlet will decrease. Combining Figs. 15(c) and 15(d), it can be found that with the decrease in equivalence ratio, mass flow rate of H_2 gradually reduces, pressure pulsation in combustor becomes more intense, and mixing becomes more uneven. For RDC dome, total pressure loss decreases as H_2 equivalence ratio decreases, and for downstream of RDC flow field, total pressure loss increases as H_2 equivalence ratio decreases.

Figure 19 displays velocity contours of different equivalence ratios at y = 15.375, 15, and 14.625 mm. It can be observed that as equivalence ratio decreases, the high-speed region in flow field gradually moves downstream. At RDC outlet, the flow field velocity reaches 350 m/s, with some regions reaching 400 m/s. Additionally, as equivalence ratio

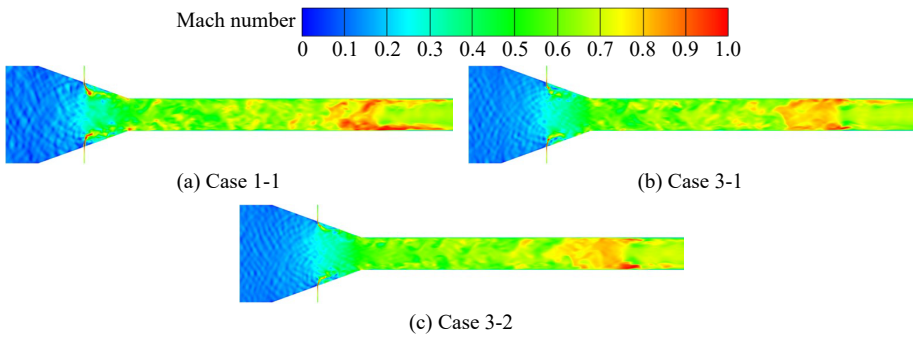

Fig. 16. Mach Number contours of different equivalence ratios.

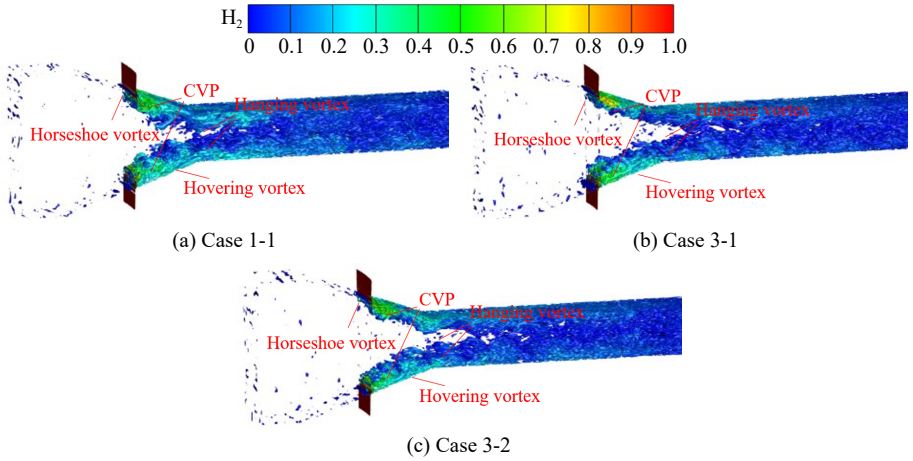

Fig. 17. H_2 mass fraction in terms of the Q-criterion isosurface ($Q = 10^{10}$) of different equivalence ratios.

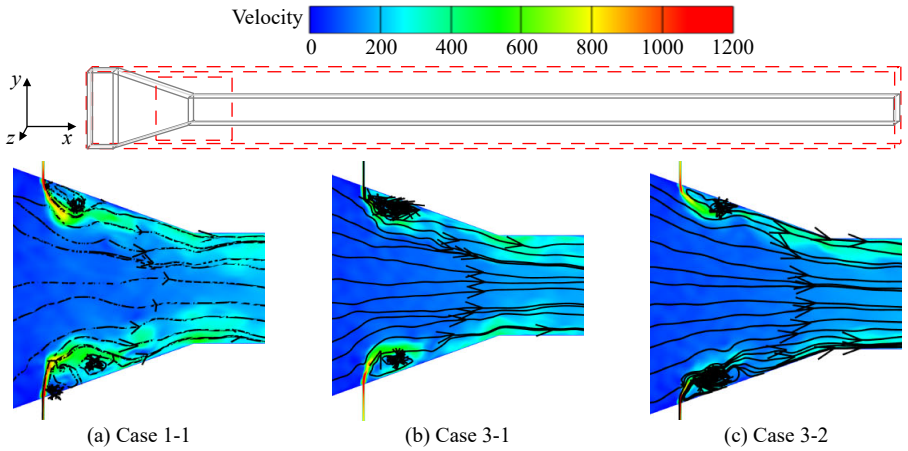

Fig. 18. Velocity streamline contours of different equivalence ratios at $z = 0$ mm.

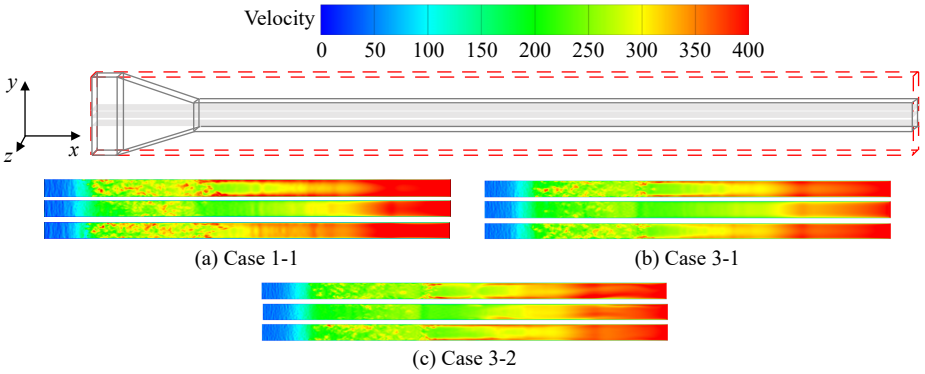

Fig. 19. Velocity contours of different equivalence ratios at $y = 15.375$, 15, and 14.625 mm.

declines, the z = 0 mm cross-section velocity of flow field rises gradually to 350 m/s, with the high-speed region moving toward RDC dome.

IV. Conclusion

(1) Compared with single channel injection, horseshoe vortices in symmetric H_2 injection configuration exhibit a scattered distribution near hydrogen annulus. Meanwhile, at axial position of $x = 3$ mm, detonation area ratio increases from 0.40 to 0.93, indicating that mixing performance of symmetric injection is superior to that of single-side injection. Symmetric H_2 injection causes the high-velocity regions of flow field to be located near inner and outer wall surfaces, which increases both mixing non-uniformity and NUP.

(2) CVPs distributed near fuel channels play a significant

role in mixing characteristics of flow field. As H_2 injection position shifts from converging section to combustor dome, mixing non-uniformity NUP and pressure loss increase gradually, detonation area ratio decreases. In the ignition zone (at x = 4.5 mm in RDC), mixing non-uniformity decreases from 5.37 to 1.68, total pressure recovery coefficient increases by 1.47%, and detonation area ratio rises from 0.318 to 0.417.

(3) Variations in equivalence ratio exert only a marginal influence on mixing non-uniformity and detonation area ratio, while also inducing a slight reduction in Mach number, a contraction of recirculation zone and a deterioration in total pressure stability. Total pressure recovery coefficient at the same cross-section decreases with decreasing equivalence ratio; however, the opposite trend is observed at axial positions after x = 3.5 mm.

Compared with single-side H_2 injection structure, symmetric H_2 injection structure offers numerous advantages, such as significantly improving detonation area ratio. However, it still has some issues in terms of total pressure recovery coefficient. Therefore, there is a potential to achieve lower total pressure loss while maintaining mixing performance by further adjusting the injection port angle, introducing a blunt body structure, and modifying the configuration of convergent section.

Declaration of competing interest

The authors declare that they have no known competing financial interests or personal relationships that could have appeared to influence the work reported in this paper.

Acknowledgements

The authors would like to acknowledge the National Natural Science Foundation of China (Grant No. 52506042) and Jilin Provincial Key Research and Development Plan Project (Grant No: 20240304091SF) for supporting this work.

Use of AI statement

During the preparation of this manuscript, the authors used an AI language tool to polish the English expression. The authors have reviewed and edited the content and take full responsibility for the final version of the manuscript.

References

[1] T. A. Kaemming and D. E. Paxson, "Determining the pressure gain of pressure gain combustion," in *2018 Joint Propulsion Conference*, 2018.

[2] P. Wolański, "Detonative propulsion," *Proc. Combust. Inst.*, vol. 34, no. 1, pp. 125–158, Jan. 2013.

[3] V. Anand and E. Gutmark, "Rotating detonation combustors and their similarities to rocket instabilities," *Prog. Energy Combust. Sci.*, vol. 73, pp. 182–234, Jul. 2019.

[4] Y. Z. Liu, X. X. Sun, V. Sethi, D. Nalianda, Y. G. Li, and L. Wang, "Review of modern low emissions combustion technologies for aero gas turbine engines," *Prog. Aerosp. Sci.*, vol. 94, pp. 12–45, Oct. 2017.

[5] J. Higashi, C. Ishiyama, S. Nakagami, K. Matsuoka, J. Kasahara, A. Matsuo, I. Funaki, and H. Moriai, "Experimental study of disk-shaped rotating detonation turbine engine," in *55th AIAA Aerospace Sciences Meeting*, 2017.

[6] A. Naples, J. Hoke, R. Battelle, and F. Schauer, "T63 turbine response to rotating detonation combustor exhaust flow," *J. Eng. Gas Turbines Power*, vol. 141, no. 2, pp. 021029, Feb. 2019.

[7] A. Lentsch, R. Bec, L. Serre, F. Falempin, E. Daniau, D. Piton, A. Prigent, G. Canteins, R. Zitoun, D. Desbordes, F. Jouot, and I. Gökalp, "Overview of current French activities on PDRE and continuous detonation wave rocket engines," in *AIAA/CIRA 13th International Space Planes and Hypersonics Systems and Technologies Conference*, 2005, pp. 258–270.

[8] Z. Liu, J. Braun, and G. Paniagua, "Thermal power plant upgrade via a rotating detonation combustor and retrofitted turbine with optimized endwalls," *Int. J. Mech. Sci.*, vol. 188, pp. 105918, Dec. 2020.

[9] X. Y. Liu, M. Y. Luan, Y. L. Chen, and J. P. Wang, "Flow-field analysis and pressure gain estimation of a rotating detonation engine with banded distribution of reactants," *Int. J. Hydrogen Energy*, vol. 45, no. 38, pp. 19976–19988, Jul. 2020.

[10] I. V. Walters, A. Lemcherfi, R. M. Gejji, S. D. Heister, and C. D. Slabaugh, "Performance characterization of a natural gas-air rotating detonation engine," *J. Propuls. Power*, vol. 37, no. 2, pp. 292–304, Mar. 2021.

[11] S. M. Frolov, V. S. Aksenov, and V. S. Ivanov, "Experimental proof of Zel'dovich cycle efficiency gain over cycle with constant pressure combustion for hydrogen-oxygen fuel mixture," *Int. J. Hydrogen Energy*, vol. 40, no. 21, pp. 6970–6975, Jun. 2015.

[12] P. Wolański, "Application of the continuous rotating detonation to gas turbine," *Appl. Mech. Mater.*, vol. 782, pp. 3–12, Aug. 2015.

[13] E. Bach, C. O. Paschereit, P. Stathopoulos, and M. D. Bohon, "An empirical model for stagnation pressure gain in rotating detonation combustors," *Proc. Combust. Inst.*, vol. 38, no. 3, pp. 3807–3814, Jan. 2021.

[14] J. P. Zhou, F. L. Song, Y. Wu, S. D. Xu, X. K. Yang, P. Cheng, and Y. H. Li, "Investigation of pressure gain characteristics for kerosene-hot air RDE," *Combust. Flame*, vol. 247, pp. 112503, Jan. 2023.

[15] J. P. Zhou, F. L. Song, Y. Wu, S. D. Xu, X. K. Yang, H. Liu, and Y. H. Li, "Investigation of pressure gain characteristics of RDE with Tesla valve inlet scheme," *Exp. Therm. Fluid Sci.*, vol. 146, pp. 110909, Aug. 2023.

[16] X. K. Yang, F. L. Song, Y. Wu, S. G. Guo, S. D. Xu, J. P. Zhou, and H. Liu, "Suppression of pressure feedback of the rotating detonation combustor by a Tesla inlet configuration," *Appl. Therm. Eng.*, vol. 216, pp. 119123, Nov. 2022.

[17] Z. T. Jiao, K. Wang, Q. Xiao, Y. H. Zhang, and W. Fan, "Characteristic velocity analysis of the total pressure gain of rotating detonation combustors," *Proc. Combust. Inst.*, vol. 40, no. 1-4, pp. 105626, Jan. 2024.

[18] J. H. Kang, F. L. Song, Y. Wu, D. C. Zhang, J. P. Zhou, and X. P. Sun, "Experimental study on the suppression of inlet blockage in rotating detonation combustor by porous-wall," *Acta Astronaut.*, vol. 225, pp. 477–488, Dec. 2024.

[19] S. Gray, M. McLoughlin, and G. Ciccarelli, "Fuel-oxygen mixing and detonation propagation in a linear rotating detonation rocket engine geometry," *Combust. Flame*, vol. 260, pp. 113250, Feb. 2024.

[20] A. P. Nair, D. D. Lee, D. I. Pineda, J. Kriesel, W. A. Jr. Hargus, J. W. Bennewitz, B. Bigler, S. A. Danczyk, and R. M. Spearrin, "Methane-oxygen rotating detonation exhaust thermodynamics with variable mixing, equivalence ratio, and mass flux," *Aerosp. Sci. Technol.*, vol. 113, pp. 106683, Jun. 2021.

[21] T. Sato, F. Chacon, L. White, V. Raman, and M. Gamba, "Mixing and detonation structure in a rotating detonation engine with an axial air inlet," *Proc. Combust. Inst.*, vol. 38, no. 3, pp. 3769–3776, Jan. 2021.

[22] T. Gaillard, D. Davidenko, and F. Dupoirieux, "Numerical simulation of a Rotating Detonation with a realistic injector designed for separate

supply of gaseous hydrogen and oxygen," *Acta Astronaut.*, vol. 141, pp. 64–78, Dec. 2017.

[23] T. Gaillard, D. Davidenko, and F. Dupoirieux, "Numerical optimisation in non reacting conditions of the injector geometry for a continuous detonation wave rocket engine," *Acta Astronaut.*, vol. 111, pp. 334–344, Jun. /Jul. 2015.

[24] Q. Y. Meng, N. B. Zhao, H. T. Zheng, J. L. Yang, and L. Qi, "Numerical investigation of the effect of inlet mass flow rates on H_2/air non-premixed rotating detonation wave," *Int. J. Hydrogen Energy*, vol. 43, no. 29, pp. 13618–13631, Jul. 2018.

[25] Q. Y. Meng, N. B. Zhao, H. T. Zheng, J. L. Yang, Z. M. Li, and F. Q. Deng, "A numerical study of rotating detonation wave with different numbers of fuel holes," *Aerosp. Sci. Technol.*, vol. 93, pp. 105301, Oct. 2019.

[26] X. Y. Xu, X. S. Wu, C. F. Zhuo, and H. Ma, "Numerical simulation of mixing characteristics in rotating detonation engine combustor," *J. Ballist.*, vol. 27, no. 3, pp. 66–75, Sep. 2015.

[27] X. Y. Xu, C. F. Zhou, X. S. Wu, J. Li, and H. Ma, "Numerical simulation of injection schemes with separate supply of fuel and oxidizer effects on rotating detonation engine," *Acta Aeronaut. Astronaut. Sin.*, vol. 37, no. 4, pp. 1184–1195, Apr. 2016.

[28] B. A. Rankin, C. A. Fugger, D. R. Richardson, K. Y. Cho, J. L. Hoke, A. W. Caswell, J. R. Gord, and F. Schauer, "Evaluation of mixing processes in a non-premixed rotating detonation engine using acetone PLIF imaging," in *54th AIAA Aerospace Sciences Meeting*, 2016.

[29] R. Driscoll, A. St. George, and E. J. Gutmark, "Numerical investigation of injection within an axisymmetric rotating detonation engine," *Int. J. Hydrogen Energy*, vol. 41, no. 3, pp. 2052–2063, Jan. 2016.

[30] R. Driscoll, A. St. George, V. Anand, S. Randall, and E. J. Gutmark, "Numerical investigation of inlet injection in a rotating detonation engine," in *53rd AIAA Aerospace Sciences Meeting*, 2015.

[31] R. Driscoll, P. Aghasi, A. St George, and E. J. Gutmark, "Three-dimensional, numerical investigation of reactant injection variation in a H_2/air rotating detonation engine," *Int. J. Hydrogen Energy*, vol. 41, no. 9, pp. 5162–5175, Mar. 2016.

[32] S. Weiss, M. D. Bohon, C. O. Paschereit, and E. J. Gutmark, "Computational study of reactants mixing in a rotating detonation combustor using compressible RANS," *Flow Turbul. Combust.*, vol. 105, no. 1, pp. 267–295, Jun. 2020.

[33] N. Ben Ali, A. Basem, P. Ghodratallah, P. K. Singh, D. J. Jasim, K. T. Falih, M. Ahmed, A. Eladeb, L. Kolsi, and A. S. El-Shafay, "Computational study of the coaxial air and fuel jet through a 3-lobe strut injector for efficient fuel mixing in a supersonic combustion chamber," *Energy*, vol. 311, pp. 133276, Dec. 2024.

[34] D. T. Chong, Y. P. Bai, Q. B. Zhao, W. X. Chen, J. J. Yan, and Y. B. Hong, "Direct numerical simulation of vortex structures during the late stage of the transition process in a compressible mixing layer," *Phys. Fluids*, vol. 33, no. 5, pp. 054108, May 2021.

[35] W. Huang, Z. B. Du, L. Yan, and Z. X. Xia, "Supersonic mixing in airbreathing propulsion systems for hypersonic flights," *Prog. Aerosp. Sci.*, vol. 109, pp. 100545, Aug. 2019.

[36] C. Sun, M. Barzegar Gerdroodbary, A. M. Abazari, S. Hosseini, and Z. X. Li, "Mixing efficiency of hydrogen multijet through backward-facing steps at supersonic flow," *Int. J. Hydrogen Energy*, vol. 46, no. 29, pp. 16075–16085, Apr. 2021.

[37] Y. C. Li, M. Barzegar Gerdroodbary, R. Moradi, and H. Babazadeh, "The influence of the sinusoidal shock generator on the mixing rate of multi hydrogen jets at supersonic flow," *Aerosp. Sci. Technol.*, vol. 96, pp. 105579, Jan. 2020.

[38] L. Qi, L. Fu, S. Z. Liu, X. J. Niu, and W. P. Hong, "Investigation on mixing characteristics of rotating detonation combustor with convergent inlet," *Int. J. Hydrogen Energy*, vol. 72, pp. 573–587, Jun. 2024.

[39] R. Zhou, B. L. Tian, X. P. Li, and J. P. Wang, "Large eddy simulation of mixing characteristic in the cold rotating detonation chamber," in *31st International Symposium on Shock Waves 2*, A. Sasoh, T. Aoki, and M. Katayama, Eds. Cham: Springer, 2019, pp. 105–112.

[40] M. J. Zhao and H. W. Zhang, "Large eddy simulation of non-reacting flow and mixing fields in a rotating detonation engine," *Fuel*, vol. 280, pp. 118534, Nov. 2020.

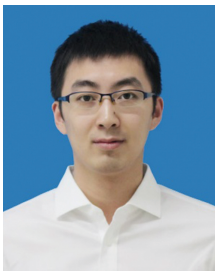

Lei Qi graduated from Harbin Engineering University. He is currently an Associate Professor and Master's Supervisor in the Department of Basic Teaching, School of Energy and Power Engineering, Northeast Electric Power University. His research interests include detonation combustion propulsion technology, gas turbine combustors, and novel power cycles.



Guangyao Li is currently a graduate student majoring in Power Engineering and Engineering Thermophysics at the School of Energy and Power Engineering, Northeast Electric Power University.



Lei Fu is currently a graduate student majoring in Power Engineering and Engineering Thermophysics at the School of Energy and Power Engineering, Northeast Electric Power University. He was awarded the title of Outstanding Graduate of Zhejiang Province in 2022 during his undergraduate studies and won the National Scholarship during his postgraduate period.



Wenpeng Hong, Ph.D., Professor, Doctoral Supervisor, School of Energy and Power Engineering, Northeast Electric Power University. He is a young and middle-aged professional and technical talent with outstanding contributions in Jilin Province, a member of the Energy and Power Engineering Teaching Steering Committee of the Ministry of Education, a member of the Energy and Power Engineering Discipline Teaching Committee of the China Electric Power Education Association, a council member of the Chinese Society of Power Engineering, a member of the Thermal Science and Engineering Professional Committee of the China Energy Research Society, and an editorial board member of the Journal of Northeast Electric Power University and Power Generation Technology.



Haoshu Ding holds a Ph.D. degree in Engineering. She is a Lecturer (appointed as Associate Professor by the university) and Master's Supervisor in the Department of Basic Teaching, School of Energy and Power Engineering, Northeast Electric Power University. Her research interests include low-carbon restructuring of energy materials and systems and thermal conversion and resource utilization of organic solid waste.



Xiaojuan Niu, Associate Professor, Ph.D. in Engineering, Master's Supervisor, School of Energy and Power Engineering, Northeast Electric Power University. She graduated from the State Key Laboratory of Multiphase Flow in Power Engineering at Xi'an Jiaotong University in 2018. Her research mainly focuses on multiphase flow and heat transfer, performance evaluation of supercritical CO_2 novel power cycle systems, and novel energy storage systems. She has presided over one Youth Fund Project of the National Natural Science Foundation of China, one Excellent Young Talents Fund Project of the Science and Technology Department of Jilin Province, one General Project of the Science and Technology Department of Jilin Province, and one project of the Education Department of Jilin Province.



Guohua Wu has long been engaged in research on AI application-related technologies such as condition monitoring, fault diagnosis, and emergency decision-making. He is currently a tenured Associate Professor and Senior Engineer at Shenzhen Technology University. He serves as the Party Branch Secretary of the Sino-German Automation program, Deputy Director of the Shenzhen Nuclear Safety and Emergency Industry Science and Technology Innovation Center, Deputy Secretary-General of the Shenzhen Association of Automation, and a Young Committee Member of the Research Reactors and New Reactors Branch of the Chinese Nuclear Society, among other positions.